Ceramics International 46 (2020) 16321–16327

Contents lists available at ScienceDirect

Ceramics International

journal homepage: www.elsevier.com/locate/ceramint

Thermal coarsening of individual titanate nanowires and their assemblies: Surface vs. bulk diffusion

L. Rossi, X. Berdat, M. Spina, S. Brown, L. Bernard, S. Katrych, L. Forró, E. Horváth*

Laboratory of Physics of Complex Matter, École Polytechnique Fédérale de Lausanne, CH-1015, Lausanne, Switzerland

ARTICLE INFO

Keywords:
TiO_2
Sintering
Ostwald ripening
Hardness

ABSTRACT

The thermal coarsening of titanate nanowires was investigated from room temperature to 1000 °C by AFM, SEM, XRD and Raman spectroscopy. Phase transformation kinetics and the external morphology were studied in two configurations: i) as individual and suspended titanate nanowires on SiO_2 surface (denoted as 2D geometry); and ii) as large assembly in form of sintered pellets (denoted as 3D geometry). The individual titanates nanowires were coarsened far below the melting temperature (1843 °C) of TiO_2 and two temperature dependent geometrical transformation changes were identified. In the first one, the height decreases around 200 °C (~20% shrinkage) due to the dehydration of the layered titanate, followed by the titanate to anatase recrystallization until 600 °C. Interestingly, the surface area of the SiO_2 supported high temperature stabilized individual nanowires increased or remained constant, which may be due to the topotactic effects and epitaxial strain stabilization. In the second one, at sintering temperature of 600–1000 °C, an intense nanowire coarsening was observed driven by a surface diffusion mechanism on substrate and a surprising stabilization of the anatase TiO_2. In the case of a 3D assembly of the nanowires the densification with significant particle coarsening is accompanied by the phase transformation from anatase to rutile around the known phase transition temperature. These results suggest that the surface area evolution of individual titanium oxide nanowires on SiO_2 appreciably differs from the 3D assembly, and the surfaces may induce an extra stabilization effect and deviation from the classical Ostwald ripening surface diffusion model.

1. Introduction

Among different semiconductor oxides, titanium dioxide continues to attract considerable theoretical and experimental attention because of its technological relevance in applications such as environmental purification [1,2], solar energy harvesting [3], memristors [4], catalysis [5], advanced ceramic materials and more. Different allotropes and morphologies of the compound are being examined. The former most commonly are the anatase and rutile phases [6], while the latter include millimeter sized single crystals [7], polycrystalline sintered ceramics [8], thin films as well as isotropic and anisotropic micron and nano-sized particles [9,10]. In most of the applications, titania is used as a nanoparticle-based coating, deposited by blading, spin coating, spraying or sol-gel techniques [11,12]. A subsequent heat treatment is often required in order to increase the crystallinity and integrity of these functional coatings. During the thermal treatment, the differences in the thermal expansion of the support materials may cause additional stresses that can lead to the detaching or overall failure of the mesoporous film. Much has been learnt from recent studies of the coarsening behavior of TiO_2 nanostructures of nearly spherical, isotropic nanoparticles. Indeed, the degree of the particle anisotropy can induce important shape-dependent variation in properties of the material, which raises the question how the coarsening of anisotropic particles proceeds at the interfaces and in the bulk ($\geq$100 nm from the interface).

For these reasons, studying the kinetics of the thermal coarsening of the elongated titanates is fundamentally important to control its structural, electronic and mechanical properties essential for special applications as thermal super insulators [13], magnetism [14,15], photocatalysis [16] and self-cleaning surfaces [17], photodetectors [18], fiber polymer reinforcement [19], biofunctionalized nanocarriers [20–22], humidity [23] and ph [24] sensors and mesoscopic solar cells [8].

The aim of this study is to shed light on the temperature dependent structural and geometrical evolution of suspended individual titanate nanowires or individual nanowires deposited on a substrate, called 2D geometry, and of assembly of nanowires, called 3D geometry. We used various complementary techniques such as Scanning Electron Microscope (SEM), Atomic Force Microscope (AFM), Raman Spectroscopy and X-Ray

* Corresponding author. EPFL SB IPHYS LPMC, PH D2 445 (Bâtiment PH), Station 3, CH-1015, Lausanne, Switzerland.
E-mail address: endre.horvath@epfl.ch (E. Horváth).

https://doi.org/10.1016/j.ceramint.2020.03.189
Received 3 February 2020; Received in revised form 17 March 2020; Accepted 18 March 2020
Available online 22 March 2020

Diffraction (XRD), which have allowed us to identify some unexpected differences in the phase stabilization and surface diffusion behavior of the 2D and 3D assemblies.

2. Experimental

2.1. Material synthesis

Protonated titanate nanowires ($H_2Ti_3O_7$) were prepared by a two-step hydrothermal process; the typical synthesis procedure is described in Refs. [8]. Our nanowires have a high aspect ratio in cross section, therefore the term nanobelts would be more appropriate. However, for consistency with previous literature we refer to them as nanowires [25].

2.2. Preparation of 2D system

Individual titanate nanowires are deposited from an ultrasonicated suspension via a stamping method. The nanowire suspension was first filtered on a Teflon membrane with pores sizes 0.45 μm and subsequently stamped against the silicon substrate for 1 min. After that the Teflon membrane was removed and the well separated titanate nanowires remains on the silicon substrate due to the surface adhesion differences between silicon and Teflon.

2.3. Preparation of 3D pellets

Titanate powder was loaded into a graphite die (diameter 20 mm) and sintered via spark plasma sintering (SPS) under 50 MPa pressure. Sintering is performed with a heating rate of 50 °C/min with a 2 min dwell at the target temperature.

For the Vickers hardness test a commercial Sigma Aldrich anatase TiO_2 white powder was used; sintering procedure is given elsewhere in Refs. [13].

2.4. Characterization

Scanning electron microscope (Zeiss Merlin, Gemini II column) was employed to observe the morphology of single nanowires and pellets. SEM images were acquired at an accelerating voltage of 2 kV and 150 pA electron beam current. The phase composition was investigated using an X-ray diffractometer (Empyrean system equipped with a PIXcel-1D detector in Bragg-Brentano geometry, Cu Kα radiation). The surface topography of the nanowires was investigated using an atomic force microscope (AFM, Park Systems). We used NCLR Park tips in non-contact mode; the tip radius was 10 nm and the force constant was 48 N/m.

Raman spectroscopy was performed with a confocal Raman spectrometer from Horiba Scientific company, the LabRam HR, using a 532 nm laser and a 100× objective lens (0.3 μm spot size). The hardness was measured by Vickers indentation technique (Shimadzu) on polished surfaces of the TiO_2 pellets with a Vickers indenter and a load of 0.5 kg for 12 s.

3. Results and discussion

Thin films of titanate nanowires were prepared by wet-chemical method. $H_2Ti_3O_7$ based porous films with thicknesses of 10 and 70 μm were fabricated on technologically relevant conductive glass substrate coated with F-doped (FTO) by doctor blading method. In order to promote the phase transformation from titanate into TiO_2 anatase phase, crystalline structures of which are shown in Fig. 1a, the resulting porous coatings were annealed at 500 °C in air. Fig. 1b shows the representative photographs and the corresponding top-view surface morphologies imaged by SEM. Despite the fact that the same deposition technique and annealing process was used for both layers, failures such as peeling can be observed in the case of thicker, 70 μm thick film. Top-view SEM micrographs confirm that the adhesion quality of the films to the FTO substrate was dissimilar after the sintering. Plenty of cracks 50–200 μm in length formed on the surface of the thicker layer, while uniform and flat surface with no observable cracks was characteristic for the 10 μm thick layer.

The top-view SEM graphs (Fig. 1c) taken before and after the sintering process confirm that the thinner, 10 μm thick film was well attached to the FTO glass. It is noteworthy, that the titanate to anatase recrystallization induced about 30% shrinkage in the film thickness (Fig. 1c, inset). This observation was further confirmed by series of alpha step measurements (Fig. 1c, inset). These findings precisely portray that the sharp interface between the two dissimilar materials might be the weakest point in the system. As mentioned before, these stresses may result from the different thermomechanical properties of the two materials being combined and processed. If the relative deformations between the layers occur before the material fracture toughness increases to the level sufficient to withstand the stresses, the composite will not be able to undergo a crack-free consolidation. However, the susceptibility of the interfaces to these types of failures is influenced by more than just the differences in the thermomechanical properties of the combined materials. Geometrical effects such as sharp corners, heating and cooling rate, particle size and shape, particle size distribution, orientation of the particles, porosity, degree of crystallinity and crystal phase change could have a significant role on eventual crack formation and propagation between the adjacent layers. Many studies have been reported that, during the thermal annealing of elongated titanates, the material can undergo transitions to several crystalline phases such as TiO_2(B), $Na_2Ti_3O_7$, anatase, rutile [26–28], depending on the annealing temperature and phase purity of the starting material.

In order to understand the sintering behavior of elongated titanate-based 3D coatings, we decided to study the temperature dependent structural and geometrical evolution of its building “bricks”, the individual titanate nanowires, and compared it to the behavior of the sintered films.

3.1. Analysis of 2D system

We have measured the dimensional change of 21 individual nanowires under repetitive annealing in air, increasing temperature by 200 °C at each step, going from room temperature up to 1000 °C.

The changes in height were measured by means of AFM, while SEM images allowed us to quantify length and width variations. The dimensional variations such as, the cross section and contact surface area and total volume after each annealing step are summarized in Fig. 2. Fig. 2a shows the SEM and AFM images of two nanowires close to each other taken as deposited (RT), after heat treatments at 600 °C and 800 °C.

During the heat treatment from RT to 200 °C, the average nanowire height is reduced by 18.7%, while negligible change in the length and width was observed. At the annealing temperatures of 400 °C and 600 °C, the average height reduction was 20.9% and 23.7% respectively. Again, no change in the width and length has been observed as compared to the original room temperature values. At higher temperatures (above 600 °C), drastic changes in all the dimensions of the nanowire occurred. Annealing temperature of 800 °C caused significant nanowire enlargement in the plane of the substrate (Fig. 2c). The average height was drastically reduced down to 20% of the RT value, accompanied by a pronounced change observed in the average nanowire width, which became four times larger as compared to the original value. However, the length slightly increased by 4%. The total volume of nanowires remained roughly constant, see Fig. 2c.

These results allow us to identify two annealing temperature dependent geometrical phase transformations of nanowires, hereafter called phase change 1 (TTA-Titanate to Anatase recrystallization from

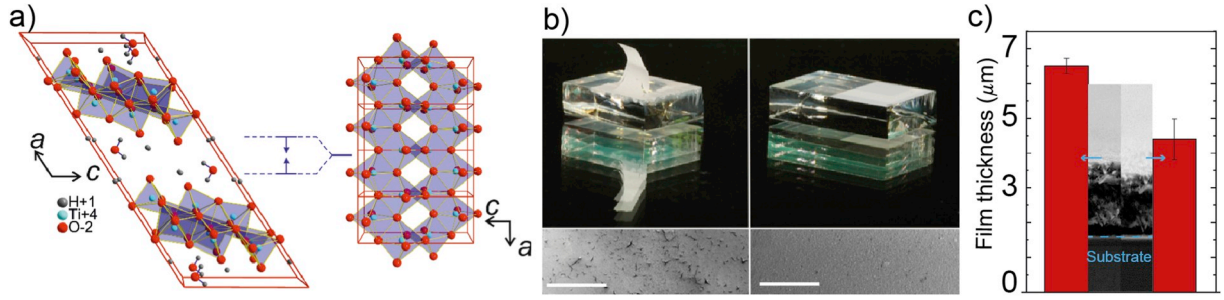

Fig. 1. a) Titanate to anatase crystallization; b) Titanate films of 70 and 10 μm (from left to right) and the respectively SEM morphology, the scale bars correspond to 1 mm; c) Film thickness before and after the sintering and the corresponding profile (inset).

RT to 600 °C) and phase change 2, which are indicated by the dashed vertical lines in Fig. 2c. The size change in phase change 2 is driven by diffusion mechanism typical of our nanowires.

In phase change 1, significant shrinking of the height occurred, while the length and width remained constant indicating minimal to no surface diffusion happened.

Indeed, the as deposited nanowires possess a layered structure composed of titanium centered octahedra and can be indexed as monoclinic $H_2Ti_3O_7$. In between the layers a relatively large gallery spacing of 0.6–0.8 nm has been determined from High Resolution-Transmission Electron Microscopy (HR-TEM) and XRD measurements [29]. Here, various positively charged cations stabilize the structure, depending on the applied synthesis and post synthesis procedure (ion-exchange). The physiosorbed and chemisorbed water, (e.g. the hydrate shell of the balancing cations as well as the titanium centered octahedra build host layer) accounts for a significant H_2O content of the material. As a consequence, the one-dimensional shrinkage at 200 °C can be simply explained by the loss of loosely bound water adsorbed on the surface and in between the gallery spacing of the titanate layers. Further annealing leads to loss of strongly bound structural crystalline water followed by the titanate to anatase recrystallization. For ascertaining the experimental results we compared the volumetric parameters of the unit cells of the monoclinic protonated titanate $H_2Ti_3O_7$ and the resulting TiO_2 anatase phase (see Fig. 1a for the crystallographic representation of the two phases). In our calculation the number of Ti atoms in the two compounds was kept constant. The theoretical volumetric reduction in the trititanate-anatase transformation found to be 20%. Hence, this theoretical value was in a good agreement with the experimental observations.

Following phase change 2, a thermally activated anomalous particle coarsening was observed. The nanowire height decreased drastically. In parallel, the width and length increased significantly, resulting in about a factor of 4 increase in the nanowire-support contact area. Since, the annealing temperature was far below the melting point of titania (1843 °C) the substantial change in the shape of the elongated particles is ascribed to a surface diffusion process. Taking the geometrical

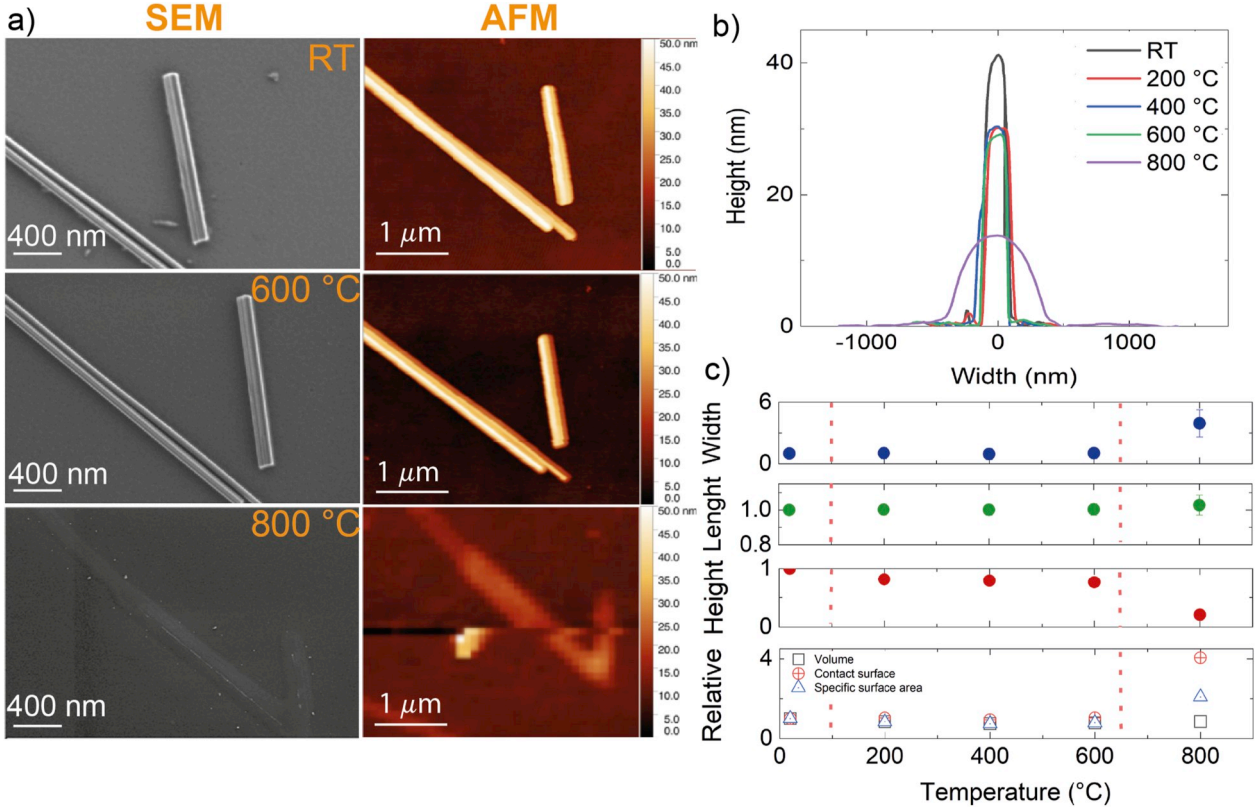

Fig. 2. a) SEM and AFM of two nanowires close to each other, just after deposition, after 600 °C and 800 °C heat treatment. Statistic of geometrical parameters of single fibers on a SiO_2 substrate after different heat treatment; b)Nanowire cross section; c) Relative change from initial value of all three dimensions and the total volume, the contact surface area and the specific surface areas: the vertical dashed lines separates the three particle coarsening regimes.

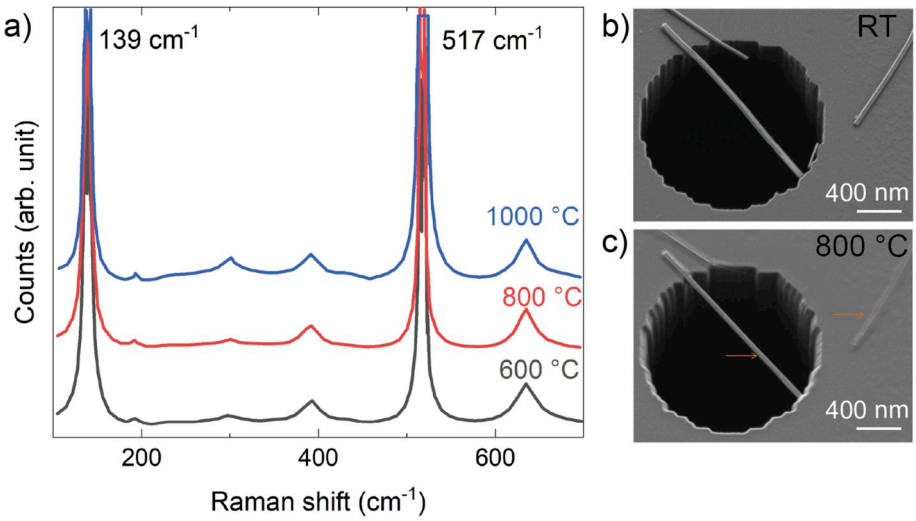

Fig. 3. a) Raman spectroscopy of an individual nanowire at 600, 800 and 1000 °C heat treatment; b) SEM of a nanowire suspended over a microfabricated hole at room temperature; c) SEM of the same nanowire after heat treatment at 800 °C in air.

parameters measured by AFM and SEM the surface area change of individual nano-objects has been determined from Fig. 2b and c.

Based on the classical Ostwald ripening model, it was expected, that upon elevating the annealing temperature the surface area of the nanoparticles will systematically decrease. This was actually verified for the phase transition 1 where the surface area decreased by a few percent, driven by the 20% reduction of the height while keeping the other dimensions almost constant. However, we found out that following the phase change 2, passing from 600 °C to 800 °C annealing temperature, the surface area of the nanowires increased by 200%. This unexpected behavior of the surface area appreciably differs from the classical Ostwald ripening surface diffusion model, where the system tries to reduce its surface area to reach a thermodynamically more stable configuration. The direction of the titanium oxide migration was found to be independent of the orientation of SiO_2 surface, hence the measured diffusion path lengths were identical in all the directions.

We have further investigated this phenomenon via Raman spectroscopy. The spectral lines versus Raman shift measured on samples submitted to different annealing temperatures, 600, 800 and 1000 °C are plotted in Fig. 3a. The perfect overlapping of the spectra taken at low and high temperatures clearly indicates that the elongated fibers remains in the metastable anatase phase without transformation to the thermodynamically expected rutile phase. This means that in these individual wires, the anatase phase can remain stable up to 1000 °C and the increase of the width, with increase of the surface area is driven by titanium oxide diffusion mechanism at the contact surface with the surface. Surface wettability and topotactic effects, such as epitaxial strain [30,31], may have important roles in the metal stable phase stabilization.

The surface diffusion mechanism is clearly recognizable and visualized in SEM images of Fig. 3b and c. In Fig. 3b, the SEM micrograph depicts nanowires on SiO_2 surface and one nanowire suspended over a microfabricated hole. Fig. 3c shows the same zone on the chip after a heat treatment at 800 °C in air. The fibers in contact with the surface show substantial increase in width and the contact area due to a surface diffusion mechanism. Interestingly, in the case of the suspended nanowire, the area in contact with the surface grew, however, the suspended part maintained its dimensions, and actually experienced a 10% reduction in width. This indicates that the coarsening and diffusion of anatase in nanowire form is highly prohibited in the absence of a substrate.

3.2. Analysis of 3D system

In this section we report the investigation on titanate nanowire coarsening in the absence of surface effects. We prepared various 3D assemblies, for instance porous pellets having 1.5–2 mm thickness, via SPS method. Based on the XRD and SEM data, coarsening effects similar to the ones observed in nanowires can be identified. In the phase change 1 (TTA-Titanate to Anatase recrystallization from RT to 600 °C, sample in Fig. 4a, the loss of crystalline water followed by the titanate to anatase recrystallization was taking place, as it is shown in Fig. S1 and as inferred by the disappearance of the $2\Theta = 10^{\circ}$ peak, originated from the gallery spacing in the layered titanate [29]. The characteristic anatase diffraction peaks appeared after annealing at 500 °C (Fig. 4 c) with the most intense peak at $2\Theta = 25.2^{\circ}$ (101). Further annealing to 600 and 700 °C resulted in an increase and narrowing of the intensities of this at 2Θ, indicating the grain growth and crystallinity increase of anatase crystallites. Most importantly, the elongated particle shape was well preserved, as it can be seen in the SEM picture of Fig. 4a. These combined results of XRD and SEM measurements suggest “surface-assisted” and “bulk” titanate nanowire coarsening in the anatase phase, similar to what happens for single nanowires. Roughly, the suggested scenario is as follows: significant shrinking in the direction perpendicular to the titanate (200) crystallographic plane occurs; at the contact points merging of aligned particles occurs via recrystallization. This titanate to anatase transformation we observed is good agreement with previous literature [32–34].

Increasing the heat treatment temperature to 900 °C the loss of the elongated fibers morphology was observed (Fig. 4b). In addition, above 900 °C the newly formed rutile phase $2\Theta = 27.5^{\circ}$ appeared, coexisting with a low amount of anatase and TiO_2 (B) phase. This was also confirmed by the Raman spectroscopy measurements reported in Fig. 4d. Above 900 °C the nanowires assembled in the pellets were transformed into a dense, nearly isotropic crystallite based sintered body. The crystallite size increased considerably: between 500 and 700 °C the crystallite size is $< z > = 23.5 \pm 3$ nm, while between 900 and 1300 °C we measured $< z > = 78.3 \pm 4$ nm. This grain evolution can be attributed to the simultaneous effects of neck formation, surface diffusion, grain coarsening and pore pinning mechanism already studied in many systems both theoretically and practically [35–42]. This 3D coarsening behavior at high temperature, above 900 °C, is quite different from the one observed in the 2D system, where no rutile phase

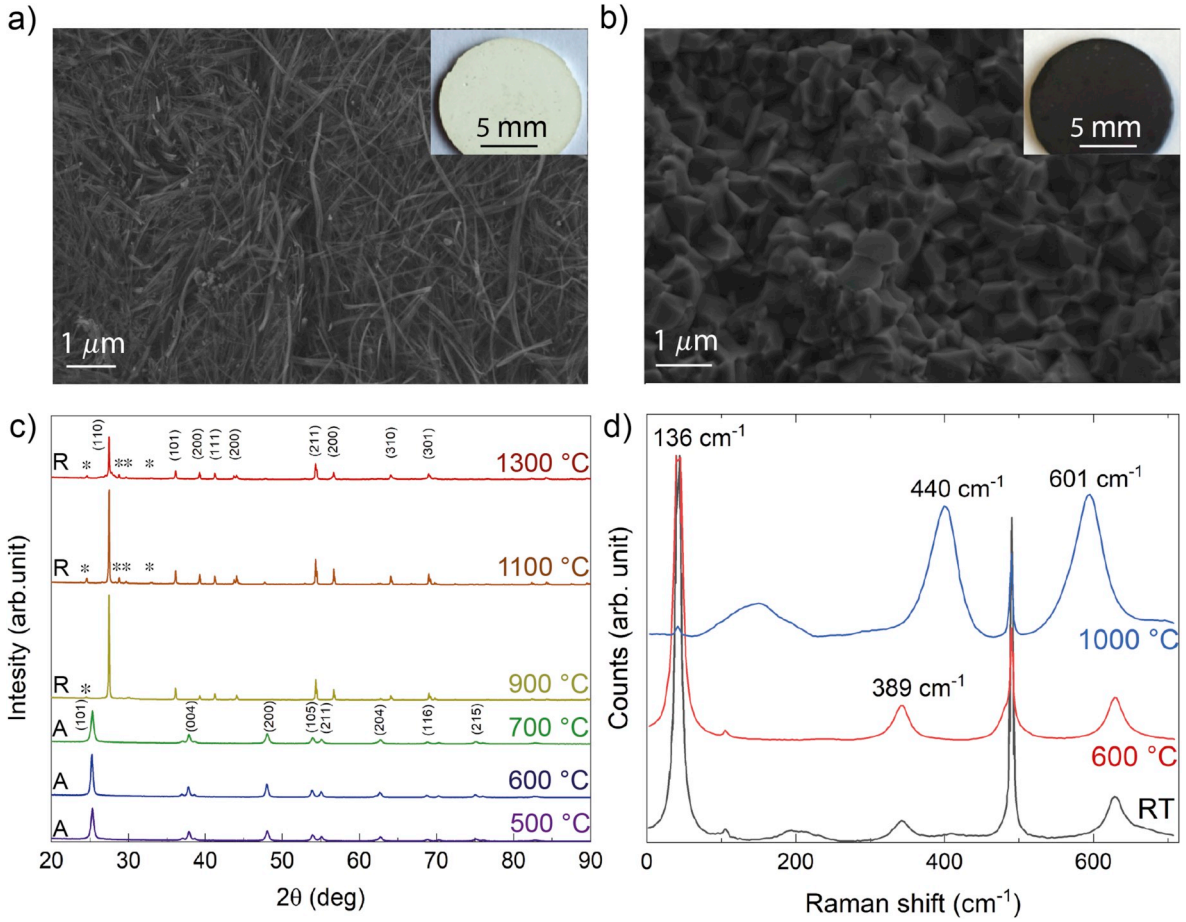

Fig. 4. a) SEM micrograph of a TiO_2 pellet sintered at 600 °C (inset TiO_2 pellet sintered at 500 °C); b) Cross section of a TiO_2 pellet sintered at 900 °C (inset TiO_2 pellet sintered at 900 °C); c) Raman spectroscopy of a pellet at room temperature, at 600 °C and 1000 °C heat treatment; d) XRD of TiO_2 pellets sintered from 500 °C till 1300 °C. "A" is for anatase, "R" for rutile phase and the * corresponds to TiO_2 (B).

appeared, and the stabilization of the metastable anatase phase occurred at reasonably high temperature. We believe these marked differences are due to the interaction between titanium oxide nanowires with the SiO_2 substrate, which plays a dominant role in the unusual high temperature stabilization of the 2D system and is absent in the coarsening mechanism of 3D pellets.

Since the activation energy, surface wettability at high temperatures and topotactic effects strongly depend on the physicochemical properties as well as the crystallographic orientation of the matter, further studying the titanium oxide-support interfaces (metal, metal oxide etc.) is mandatory for the improvement of the TiO_2 based devices.

3.2.1. Hardness vs. porosity measurement of nanowires pellets

The micro hardness values of the 3D nanowire pellets annealed at 600 °C, having a single-phase anatase composition and altered porosity were measured by Vickers method (Fig. 5). The hardness values of the sintered titania nanowires increases with decreasing porosity. For the anatase simples sintered at 600 °C the hardness of 115 HV (44% porosity) has increased to 372 HV (37% porosity). After sintering at 900 °C we measured 941 HV (1.6% porosity), isotropic particle shape and rutile phase was detected; this hardness value is in the range of the single crystal values 894-974 HV [43]. Interestingly, comparing the hardness of anatase nanowire fiber pellets to a sample having identical porosity, but instead composed of nearly spherical anatase grains, 50% higher values of hardness were observed (Fig. 5).

We believe that the beneficial role of elongated particle shape

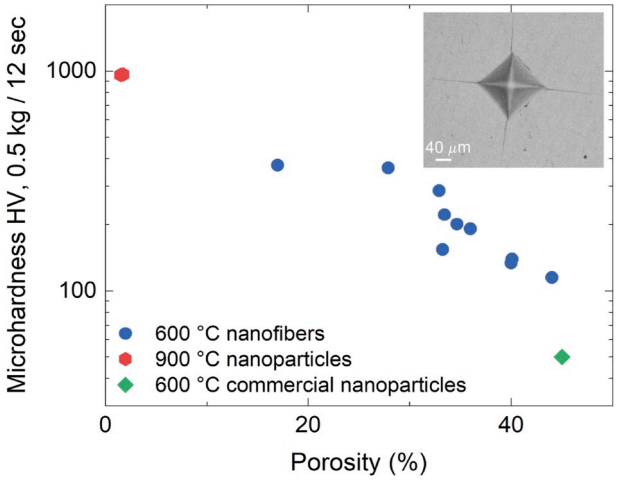

Fig. 5. Vickers microhardness vs. porosity of 3D TiO_2 nanowire pellets sintered at 600 °C and 900 °C. Inset shows typical Vickers trace on the ceramics samples. Cracks along the diagonals evidence the typical ceramic behavior of the sintered pellets.

together with coarsening effects, such as high quality grain boundary formation during sintering greatly contribute to these high hardness values and will open up the fabrication of nanowire reinforced ceramic sintered bodies.

4. Conclusion

We have investigated the coarsening behavior of suspended and surface deposited single crystalline titanate ($H_2Ti_3O_7$) nanowires as compared to their 3D assemblies. Two temperature dependent geometrical transformation phase changes were identified both for single nanowire on substrate (2D system) and for nanowire pellets (3D). During the first phase change (titanate to anatase recrystallization, above 200 °C and up to 600 °C) significant shrinking of the height of the nanowire was observed. During the second regime, at sintering temperature of 600–1000 °C an anomalous coarsening manifested as an increasing surface area of the surface deposited individual nanowires. In addition to the strong surface effects, in the 2D system, we noticed an uncommon stabilization of the metastable anatase phase and the absence of rutile phase above 900 °C. In contrast, for 3D assembly of nanowires, from 600 °C, the classical Ostwald ripening particle coarsening was observed, accompanied by a typical anatase to rutile phase transition at 900 °C.

The micro-hardness values of the sintered anatase nanowire pellets decreased with increasing porosity and showed higher hardness values as compared to sintered bodies composed of nearly spherical nanoparticles.

These results will contribute to the fabrication of novel, mechanically more stable titanium oxide nanowire-based coatings and 3D functional ceramics, which is a prerequisite for safer and durable potential products.

Declaration of competing interest

The authors declare that they have no known competing financial interests or personal relationships that could have appeared to influence the work reported in this paper.

Acknowledgments

E.H. is grateful for the support of the Swiss-African Research Cooperation (SARECO). L.R and E.H. would like to gratefully acknowledge Dr. L. Boilet, Dr. J-P Erauw and V. Dupont from Belgian Ceramic Research Centre (BCRC) for SPS experiments and discussions. L.R. also thank Dr. D. Mari for the access of Vickers hardness equipment and Dr. K. Semeniuk for discussions and revision of the manuscript. We would like to thank the Interdisciplinary Center for Electron Microscopy (CIME) at EPFL for providing SEM facilities.

Appendix A. Supplementary data

Supplementary data to this article can be found online at https://doi.org/10.1016/j.ceramint.2020.03.189.

References

[1] S. Malato, P. Fernández-Ibáñez, M.I. Maldonado, J. Blanco, W. Gernjak, Decontamination and disinfection of water by solar photocatalysis: recent overview and trends, Catal. Today 147 (2009) 1–59, https://doi.org/10.1016/j.cattod.2009.06.018.
[2] A. Fujishima, K. Hashimoto, T. Watanabe, TiO2 Photocatalysis: Fundamentals and Applications, Bkc, Tokyo, 1999.
[3] B. O'Regan, M. Grätzel, A low-cost, high-efficiency solar cell based on dye-sensitized colloidal TiO 2 films, Nature 353 (1991) 737–740, https://doi.org/10.1038/353737a0.
[4] D.B. Strukov, G.S. Snider, D.R. Stewart, R.S. Williams, The missing memristor found, Nature 453 (2008) 80–83, https://doi.org/10.1038/nature06932.
[5] J.H.A. Martens, R. Prins, H. Zandbergen, D.C. Koningsberger, Structure of rhodium/titania in the normal and the SMSI state as determined by extended x-ray absorption fine structure and high-resolution transmission electron microscopy, J. Phys. Chem. 92 (1988) 1903–1916, https://doi.org/10.1021/j100318a041.
[6] D.A.H. Hanaor, C.C. Sorrell, Review of the anatase to rutile phase transformation, J. Mater. Sci. 46 (2011) 855–874, https://doi.org/10.1007/s10853-010-5113-0.
[7] L. Forro, O. Chauvet, D. Emin, L. Zuppiroli, H. Berger, F. Lévy, High mobility n-type charge carriers in large single crystals of anatase (TiO2), J. Appl. Phys. 75 (1994) 633–635, https://doi.org/10.1063/1.355801.
[8] N. Tétreault, E. Horváth, T. Moehl, J. Brillet, R. Smajda, S. Bungener, N. Cai, P. Wang, S.M. Zakeeruddin, L. Forró, A. Magrez, M. Grätzel, High-efficiency solid-state dye-sensitized solar cells: fast charge extraction through self-assembled 3D fibrous network of crystalline TiO2 nanowires, ACS Nano 4 (2010) 7644–7650, https://doi.org/10.1021/nn1024434.
[9] J. Jaćimović, E. Horváth, B. Náfrádi, R. Gaál, N. Nikseresht, H. Berger, L. Forró, A. Magrez, From nanotubes to single crystals: Co doped TiO2, Apl. Mater. 1 (2013) 032111, , https://doi.org/10.1063/1.4820438.
[10] H. Mehranpour, M. Askari, M.S. Ghamsari, H. Farzalibeik, Study on the phase transformation kinetics of sol-gel drived nanoparticles, J. Nanomater. (2010), https://doi.org/10.1155/2010/626978.
[11] V.K. LaMer, R.H. Dinegar, Theory, production and mechanism of formation of monodispersed hydrosols, J. Am. Chem. Soc. 72 (1950) 4847–4854, https://doi.org/10.1021/ja01167a001.
[12] J. Turkevich, P.C. Stevenson, J. Hillier, A study of the nucleation and growth processes in the synthesis of colloidal gold, Discuss. Faraday Soc. 11 (1951) 55–75, https://doi.org/10.1039/DF9511100055.
[13] X. Mettan, J. Jaćimović, O.S. Barišić, A. Pisoni, I. Batistić, E. Horváth, S. Brown, L. Rossi, P. Szirmai, B. Farkas, H. Berger, L. Forró, Tailoring thermal conduction in anatase TiO 2, Commun. Phys. 2 (2019) 1–7, https://doi.org/10.1038/s42005-019-0224-7.
[14] P. Szirmai, J. Stevens, E. Horváth, L. Ćirić, M. Kollár, L. Forró, B. Náfrádi, Competitive ion-exchange of manganese and gadolinium in titanate nanotubes, Catal. Today 284 (2017) 146–152, https://doi.org/10.1016/j.cattod.2016.11.010.
[15] P. Szirmai, E. Horváth, B. Náfrádi, Z. Micković, R. Smajda, D.M. Djokić, K. Schenk, L. Forró, A. Magrez, Synthesis of homogeneous manganese-doped titanium oxide nanotubes from titanate precursors, J. Phys. Chem. C 117 (2013) 697–702, https://doi.org/10.1021/jp3104722.
[16] P. Szirmai, B. Náfrádi, A. Arakcheeva, E. Szilágyi, R. Gaál, N.M. Nemes, X. Berdat, M. Spina, L. Bernard, J. Jaćimović, A. Magrez, L. Forró, E. Horváth, Cyan titania nanowires: spectroscopic study of the origin of the self-doping enhanced photocatalytic activity, Catal. Today 284 (2017) 52–58, https://doi.org/10.1016/j.cattod.2016.10.024.
[17] B. Náfrádi, G. Náfrádi, C. Martin-Hamka, L. Forró, E. Horváth, Superior water sheeting effect on photocatalytic titania nanowire coated glass, Langmuir 33 (2017) 9043–9049, https://doi.org/10.1021/acs.langmuir.7b01790.
[18] K. Mantulnikovs, P. Szirmai, M. Kollar, J. Stevens, P. Andricevic, A. Glushkova, L. Rossi, P. Bugnon, E. Horváth, A. Sienkiewicz, L. Forro, B. Náfrádi, Light-induced charge transfer at the $CH_3NH_3PbI_3/TiO_2$ interface - a low-temperature Photo-EPR assay, J. Phys. Photon. (2019), https://doi.org/10.1088/2515-7647/ab6276.
[19] M.T. Byrne, J.E. McCarthy, M. Bent, R. Blake, Y.K. Gun'ko, E. Horvath, Z. Konya, A. Kukovecz, I. Kiricsi, J.N. Coleman, Chemical functionalisation of titania nanotubes and their utilisation for the fabrication of reinforced polystyrene composites, J. Mater. Chem. 17 (2007) 2351–2358, https://doi.org/10.1039/B612886F.
[20] T. Szabó, V. Tóth, E. Horváth, L. Forró, I. Szilagyi, Tuning the aggregation of titanate nanowires in aqueous dispersions, Langmuir 31 (2015) 42–49, https://doi.org/10.1021/la504521e.
[21] M. Pavlovic, M. Adok-Sipiczki, E. Horváth, T. Szabó, L. Forró, I. Szilagyi, Dendrimer-stabilized titanate nanowire dispersions as potential nanocarriers, J. Phys. Chem. C 119 (2015) 24919–24926, https://doi.org/10.1021/acs.jpcc.5b08775.
[22] E. Horváth, L. Grebikova, P. Maroni, T. Szabó, A. Magrez, L. Forró, I. Szilagyi, Dispersion characteristics and aggregation in titanate nanowire colloids, ChemPlusChem (2018) 592–600, https://doi.org/10.1002/cplu.201300426@10.1002/(ISSN)2192-6506.earlycareer.
[23] E. Horváth, P. Rebernik Ribič, F. Hashemi, L. Forró, A. Magrez, Dye metachromasy on titanate nanowires : sensing humidity with reversible molecular dimerization, J. Mater. Chem. 22 (2012) 8778–8784, https://doi.org/10.1039/C2JM16443D.
[24] E. Horváth, I. Szilágyi, L. Forró, A. Magrez, Probing titanate nanowire surface acidity through methylene blue adsorption in colloidal suspension and on thin films, J. Colloid Interface Sci. 416 (2014) 190–197, https://doi.org/10.1016/j.jcis.2013.10.049.
[25] E. Horváth, L. Forró, A. Magrez, Titanium oxide aerogel composites, EP2964577A1 https://patents.google.com/patent/EP2964577A1/en, (2016) , Accessed date: 17 December 2019.
[26] M. Tournoux, R. Marchand, L. Brohan, Layered K2Ti4O9 and the open metastable TiO2(B) structure, Prog. Solid State Chem. 17 (1986) 33–52, https://doi.org/10.1016/0079-6786(86)90003-8.
[27] M. Qamar, C.R. Yoon, H.J. Oh, D.H. Kim, J.H. Jho, K.S. Lee, W.J. Lee, H.G. Lee, S.J. Kim, Effect of post treatments on the structure and thermal stability of titanate nanotubes, Nanotechnology 17 (2006) 5922–5929, https://doi.org/10.1088/0957-4484/17/24/004.
[28] D.V. Bavykin, F.C. Walsh, Elongated titanate nanostructures and their applications, Eur. J. Inorg. Chem. 2009 (2009) 977–997, https://doi.org/10.1002/ejic.200801122.
[29] E. Horváth, Á. Kukovecz, Z. Kónya, I. Kiricsi, Hydrothermal conversion of self-assembled titanate nanotubes into nanowires in a revolving autoclave, Chem. Mater. 19 (2007) 927–931, https://doi.org/10.1021/cm062413q.
[30] O.Yu Gorbenko, S.V. Samoilenkov, I.E. Graboy, A.R. Kaul, Epitaxial stabilization of oxides in thin films, Chem. Mater. 14 (2002) 4026–4043, https://doi.org/10.1021/cm021111v.
[31] B.A. Apgar, L.W. Martin, Understanding the competition between epitaxial strain and thermodynamics in TiO2: structural, morphological, and property evolution, Cryst. Growth Des. 14 (2014) 1981–1988, https://doi.org/10.1021/cg5000974.
[32] J.-N. Nian, H. Teng, Hydrothermal synthesis of single-crystalline anatase TiO2

nanorods with nanotubes as the precursor, J. Phys. Chem. B 110 (2006) 4193–4198, https://doi.org/10.1021/jp0567321.
[33] Y. Mao, S.S. Wong, Size- and shape-dependent transformation of nanosized titanate into analogous anatase titania nanostructures, J. Am. Chem. Soc. 128 (2006) 8217–8226, https://doi.org/10.1021/ja0607483.
[34] P. Wen, Y. Ishikawa, H. Itoh, Q. Feng, Topotactic transformation reaction from layered titanate nanosheets into anatase nanocrystals, J. Phys. Chem. C 113 (2009) 20275–20280, https://doi.org/10.1021/jp908181e.
[35] R.L. Penn, J.F. Banfield, Formation of rutile nuclei at anatase (112) twin interfaces and the phase transformation mechanism in nanocrystalline titania, Am. Mineral. 84 (1999) 871–876, https://doi.org/10.2138/am-1999-5-621.
[36] H. Zhang, J.F. Banfield, Phase transformation of nanocrystalline anatase-to-rutile via combined interface and surface nucleation, J. Mater. Res. 15 (2000) 437–448, https://doi.org/10.1557/JMR.2000.0067.
[37] W. Li, C. Ni, H. Lin, C.P. Huang, S.I. Shah, Size dependence of thermal stability of TiO2 nanoparticles, J. Appl. Phys. 96 (2004) 6663–6668, https://doi.org/10.1063/1.1807520.
[38] J. Li, Y. Ye, L. Shen, J. Chen, H. Zhou, Densification and grain growth during pressureless sintering of TiO2 nanoceramics, Mater. Sci. Eng. A. 390 (2005) 265–270, https://doi.org/10.1016/j.msea.2004.08.025.
[39] Y. Zhou, K.A. Fichthorn, Microscopic view of nucleation in the anatase-to-rutile transformation, J. Phys. Chem. C 116 (2012) 8314–8321, https://doi.org/10.1021/jp301228x.
[40] H. Zhang, J.F. Banfield, New kinetic model for the nanocrystalline anatase-to-rutile transformation revealing rate dependence on number of particles, Am. Mineral. 84 (2015) 528–535, https://doi.org/10.2138/am-1999-0406.
[41] A.A. Gribb, J.F. Banfield, Particle size effects on transformation kinetics and phase stability in nanocrystalline TiO2, Am. Mineral. 82 (2015) 717–728, https://doi.org/10.2138/am-1997-7-809.
[42] P. Galizia, G. Maizza, C. Galassi, Heating rate dependence of anatase to rutile transformation, Process. Appl. Ceram. 10 (2016) 235–241, https://doi.org/10.2298/PAC1604235G.
[43] R.A. Howie, J.W. Anthony, R.A. Bideaux, K.W. Bladh and M.C. Nicois handbook of mineralogy. Volume III: halides, hydroxides, oxides. Tucson (mineral data publishing), 1997. x + 628 pp. Price £67.50 (+ £3.40 postage; available in the UK via endsleigh book Co., norwich NR16 1LH). IBSN 0-9622097-0-8, Mineral. Mag. 62 (1998), https://doi.org/10.1180/minmag.1998.062.3.01 432–432.